A comparative study of the cryogenic performance of CFRP composites with polyethersulfone/epoxy blends and electrospun polyethersulfone interleaves

Othman Laban[a], Garth Pearce [a,*], Jin Zhang [a], Mohammad S. Islam [a]

[a] *School of Mechanical and Manufacturing Engineering, University of New South Wales, Sydney, NSW, 2052, Australia*

Abstract

Thermoslastic-modifers have been widely utilized to enhance the fracture toughness of epoxy resins for cryogenic applications. Interleaving is an effective technique to incorporate thermoslastic-modifers without compromising the resin's viscosity, making it feasible for large-scale manufacturing processes. This study presents a comparative analysis of the cryogenic performance of laminated fibre-reinforced composites, focusing on two different toughening approaches: utilizing electrospun polyethersulfone (PES) veils or epoxy/PES blends with varying PES loadings. The impact of PES loading on the developed phase morphology was examined using the single-edge-notch bending (SENB) tests. The particulate phase structure was formed in samples with PES content 2.5-10 phr, which transitioned to a co-continuous structure after exceeding 10 phr. At room temperature, the 15 phr epoxy/PES blend showed the most significant enhancements in the fracture toughness (K_{Ic}) and strain energy release rate (G_{Ic}) at 293 K were 72% and 168%, respectively. At cryogenic temperatures, the crack front tends to advance around, rather than through, the epoxy-rich domains in a co-continuous phase structure. Consequently, the 10 phr blend outperformed the 15 phr blend, with improvements in the order of 48% in K_{Ic} and 180% in G_{Ic}. Interleaving double cantilever beam (DCB) samples with a thin 5 μm electrospun PES veil have enhanced the Mode I critical strain energy release rate (G_{Ic}^{ini}) and the crack propagation energy (G_{Ic}^{prop}) by 76% and 33% at 293 K, respectively. The toughening effects were also present at 77 K, measuring improvements of 48% in G_{Ic}^{ini} and 24% in G_{Ic}^{prop}. The achieved toughening levels with interleaved laminates were comparable to those obtained with 7.5 phr PES-toughened laminates. The present results suggest that interleaving composite laminates offer great potential in enhancing the service lifetime of cryogenic fuel tanks.

Keywords: thermoplastic-epoxy blends; polyethersulfone; electrospinning; fracture toughness; interleaving technique; cryogenic

* Corresponding author's E-mail address: g.pearce@unsw.edu.au (Garth Pearce)

1 Introduction

The aerospace industry has a crucial need for lightweight propellant tanks that can efficiently handle energy-rich cryogenic liquids, ensuring optimal profitability by reducing fuel consumption [1]. However, the development of safe and reliable fibre-reinforced composite tanks for cryogenic applications poses a significant challenge that has yet to be fully addressed. One of the key issues lies in the heterogeneous nature of composite materials, which makes them susceptible to matrix-dominant cracking due to the mismatch in the coefficient of thermal expansion between the composite constituents [2]. This inherent property mismatch can lead to structural integrity concerns and compromise the tank's performance and safety in cryogenic environments.

Thermally stable thermoplastic-modifiers have become a common solution to enhance the toughness of epoxy resins, thereby mitigating cryogenic microcracking and extending the lifetime of propellant tanks [3]. The amorphous thermoplastics such as polyetherimide (PEI) [3-5], polyethersulfone (PES) [6-8], and polysulfone (PSU) [9-11], exhibit good miscibility with epoxy monomers and are prone to phase separation during the curing process [12]. Depending on the composition, the thermoplastic-rich phase can phase separated morphologies can be diverse, e.g., particulate, co-continuous, or phase-inverted structures [13]. Significant toughening effects have been reported by incorporating 5-15 phr of PES-modifier [6-8].

However, the use of thermoplastic-modifiers does come with drawbacks, particularly concerning the compromise of epoxy resin's rheological properties (increased viscosity), limiting their practical implementation in large-scale manufacturing processes [14, 15]. For instance, when incorporating 11 phr of PEI, the epoxy resin's viscosity increased sixfold at 100 °C, and at 25 phr, it soared to 370 times the original viscosity [4]. In another study, the viscosity of an epoxy system surged from 30 to 1000 Pa.s at 80 °C with the incorporation of 20 wt% of polyetherketone with a low viscous [16]. This rheological issue poses challenges for processing and could hinder the adoption of thermoplastic-modifiers in industrial settings.

Interleaving electrospun thermoplastic veils represents an alternative approach to achieve localized toughening effects in epoxy resin without causing significant increase in resin's viscosity [17]. In addition, when compared to thermoplastic-epoxy blends, this technique has less pronounced effects on the overall in-plane thermomechanical performance of the laminate [14, 18]. Another advantage of the electrospinning method is that nanofibres can be directly deposited onto dry fibre plies or pre-impregnated fibre tows, making it more feasible for use in filament winding processes [19].

Previous research has demonstrated that electrospun nanofibrous interleaves can lead to substantial improvements in Mode I and Mode II fracture toughness at room temperature, achieving enhancements of up to 250% and 213%, respectively [20]. However, there is a lack of understanding and knowledge regarding their toughening effects at cryogenic temperatures, particularly in comparison to the toughness enhancements achieved with thermoplastic-epoxy blends. Further investigation and reporting of cryogenic performance are needed to better understand the potential of electrospun nanofibrous interleaves for cryogenic applications and to compare their effectiveness with that of thermoplastic-epoxy blends.

The objective of this study is to assess the effectiveness of the interleaving technique in enhancing the interlaminar fracture toughness at cryogenic temperatures. The investigation begins with an analysis of the impact of a thermoplastic-modifier on improving the toughness of the bulk epoxy resin system, with a particular focus on understanding the influence of the phase-separated morphology on the material's performance. Subsequently, the electrospinning technique is employed to produce a nanofibrous veil composed of polyethersulfone (PES). A comparison is made between the Mode I fracture performance of interleaved carbon fibre-reinforced epoxy laminate and toughened laminates containing varying concentrations of the PES-modifier.

2 Experimental

2.1 Materials

An epoxy resin system, specifically designed for filament winding applications, was acquired from GMS Composites in Australia. The resin system consists of three components: bisphenol A diglycidyl ether (DGEBA, Araldite® LY1564), methyl tetrahydrophtalic anhydride curing agent (MTHPA, Aradur® 917-1), and tertiary amine co-hardener (accelerator 960-1). At 293

K, the resin system has viscosity of 575 mPa.s and has a pot-life of 85 hours. For the manufacture of composite laminates, Torayca T300 CK-12 unidirectional carbon fibre reinforcements with an areal weight of 200 gsm were utilized. The polyethersulfone (PES, Ultrason® E1010 NAT, 1.37 g/cc) needed for the study was procured from BASF in Germany. Additionally, N,N-Dimethylformamide (DMF, purity>99%), an organic solvent, was sourced from ChemSupply in Australia.

2.2 Preparation of hybrid Epoxy/PES blends

Blends of epoxy/PES with varying PES content of 0, 2.5, 5, 7.5, 10, and 15 phr were prepared and denoted hereafter as P0, P2.5, P5, P7.5, P10, and P15, respectively. PES pellets were dried at 150 °C overnight to remove any moisture content. Subsequently, the dried PES pellets were directly dissolved in the DGEBA-based epoxy precursor at 110 °C for a period of 24 hours. After the polymer blends became homogeneous, they were allowed to cool to room temperature before being mixed with 98 phr of MTHPA hardener and 3 phr of tertiary amine. The mixture was then degassed for 20 minutes to eliminate any trapped air bubbles. The mixture was transferred into silicon moulds to cast tensile and single-edge notched samples afterwards. The epoxy/PES blends were cured inside a 120 °C oven for 4 hours and then slowly cooled within the oven to reach room temperature.

The cured samples had a 4 mm notch for the single-edge-notch bending (SENB) test. The outer surfaces were polished to ensure flatness on all faces. Then the notch depth was increased to 6 mm by carefully tabbing the blunt notch front with a new pre-cooled razor blade. The final precrack length was measured accurately from the fractured surfaces of each specimen.

2.3 Preparation of electrospun PES veils

The electrospinning of nanofibrous PES veil was conducted using a Bioinicia box equipped with a horizontal injection point and a rotating collector. To prepare the polymer solution, dried PES pellets were dissolved in DMF solvent through mechanical stirring at 70 °C for 3 hours on a hotplate with mechanical stirring. A 5 ml syringe equipped with a metal syringe needle (21 Gauge) was filled with the prepared polymer solution and connected to a syringe pump. The pumping rate was set at 20 µl/min, and the needle-to-collector distance was fixed at 140 mm. During the electrospinning process, PES nanofibres were directly deposited onto a dry carbon fabric that was mounted onto the drum-collector. The rotating speed of the drum-collector was 300 rpm and the applied voltage was 20 kV. After the electrospinning process

was completed, the fabric with the deposited PES nanofibres was dried in a vacuum chamber at 100 °C overnight to ensure the evaporation of any residual DMF solvent from the electrospun PES nanofibres.

2.4 Manufacturing of composite laminates

The wet-layup technique was employed to manufacture composite laminates consisting of 16 unidirectional plies. To maintain the desired stiffness, only the mid-plane plies were impregnated with epoxy/PES blends, while the remaining plies were coated with pristine epoxy resin. In the interleaved laminate, a carbon fibre cloth with the PES-veil on one of its faces was stacked in the mid-plane of the laminate. To create a pre-crack, a 20 µm thick PTFE release film was inserted, inducing a 50 mm crack in the laminate. To ensure uniformity, a polyester peel-ply was placed on both faces of the laminate, resulting in a consistent surface texture on each side of the composite.

The laminate underwent curing in an ASC autoclave under vacuum pressure applied throughout the entire process. The curing schedule comprised three segments. Firstly, the laminate dwelled at 60 °C for one hour to facilitate the diffusion process between the PES-veil and epoxy resin. During the second segment, the cross-linking reaction commenced as the temperature increased to 120 °C and was maintained for four hours. Finally, after consolidation, the temperature was gradually reduced to 50 °C at a rate of 5 °C per minute.

Following the curing process, the composite laminates were cut into coupon specimens using the Multicam M1212 CNC routing machine. The milling tool used had a diameter of 3.175 mm, a spindle speed of 15000 RPM, a plunge rate of 500, and a feed rate of 5000 units. To minimize the possibility of inducing free-edge defects in the samples, the depth of cutting was set to increments of 0.2 mm.

2.5 Mechanical characterization

Mechanical tests at both 293 K and 77 K were conducted using an INSTRON 3369 testing machine, equipped with a 1 kN load cell attachment. To perform the cryogenic tests, the test fixtures and specimens were submerged in a liquid nitrogen (LN2) bath. Before submerging, the specimens underwent a gradual precooling process to prevent thermal shocks. Initially, the specimens were placed in a -28 °C freezer for an hour, followed by another hour in a -100 °C

chamber. These precooling steps ensured a smooth transition to the cryogenic temperatures and helped maintain the integrity of the specimens during testing.

The SENB tests were performed, in accordance with the ASTM D5045 standard, to assess the toughness of the epoxy/PES blends. The 3 point-bending fixture was used, with a span length of 50 mm between the two bottom 3 mm rollers, and an upper roller with a diameter of 6 mm. The loading rate was set to 5 mm/min and continued until a sudden drop in the applied load was observed, indicating rapid crack propagation through the width of the specimen. The fracture toughness (K_{Ic}) and the critical strain energy release rate (G_{Ic}) were calculated as follows:

$$K_{Ic} = \frac{P}{BW^{1/2}} f(x) \tag{1}$$

where P is the load at failure, B and W are the thickness and width of the specimen, respectively. The correction factor, $f(x)$, is a function of $x =$ precrack length/width.

$$G_{Ic} = \frac{\eta_e U}{B(W-a)} \tag{2}$$

where B is the sample thickness. The calibration factor, η_e, is a function of the precrack length, a, divided by the specimen's width, W. The total energy absorbed, U, was obtained by integrating the area under the recorded load-deflection curve. The expression of the specimen's thickness is B.

The Mode I critical strain energy release rate (G_{Ic}^{ini}) and the crack propagation energy (G_{Ic}^{prop}) were evaluated using the double-cantilever beam (DCB) test in compliance with the ASTM D5528 standard. The DCB specimens had dimensions of 180x20x3 mm³ and with precrack length of 50 mm. To conduct cryogenic testing, the DCB specimens were gradually precooled to -100 °C before submerging in a LN2 bath.

A preload of 3 N was initially applied to all specimens, followed by a loading rate of 1 mm/min. Throughout the test, load and displacement values were recorded at 5 mm increments in the crack propagation length. To monitor the progression of the delamination front, an RS digital microscope camera was used. The DCB test was conducted until the delamination propagated for at least 50 mm. Afterwards, the samples were unloaded at a rate of 25 mm/min to check for any asymmetrical loading effects. At least three samples were tested for each epoxy/PES blend and interleaved laminate at each testing temperature.

The modified beam theory was then employed to determine the G_{Ic}^{ini} and G_{Ic}^{prop} values, which were calculated using the following formulas:

$$G_{IC} = \frac{3P\delta}{2b(a + |\Delta|)} \quad (3)$$

where a is the delamination length, P and δ are the corresponding load and load-point deflection, respectively. b is the specimen width and Δ is a correction factor determined experimentally as a function of a.

2.6 Microscopy observations

Scanning electron microscopy (SEM) was employed to investigate the morphology of electrospun nanofibres and the fractured surfaces of coupon samples. The SEM analysis was conducted using the FEI Nova nanoSEM-230 equipment. To prepare the samples for SEM imaging, a 40 nm thick platinum coat was sputtered onto the surfaces. This platinum coat was applied using the Quorum Q300t machine and served to enhance the surface conductance, thereby allowing for the capture of high-contrast scans during SEM examination.

3 Results and discussion

3.1 Phase-separated morphologies

The toughening effect of the PES-modifier is primarily associated with the developed phase separated structures [21]. The SEM images in Figure 1 reveal the phase morphologies of P0, P2.5, and P10 specimens. The pristine epoxy samples (P0) exhibited a homogeneous phase morphology. Consequently, the fractured surfaces of P0 at both 293 K and 77 K conditions appeared smooth, indicating low dissipation of energy. The high-magnification images of P0 near the pre-crack and the end-edge demonstrate the transition from a river-pattern fracture to a smooth fracture surface. The river mark fracture is typical characteristics of brittle polymers, resulting from the interference of multiple local cracks [22]. River lines were observed in all the epoxy/PES samples after the pre-crack, irrespective of the testing temperature.

The particulate phase morphology was observed in P2.5 and P10 blends, resulting from the nucleation and growth (NG) mechanism of PES particulates once they surpassed the thermodynamic barrier. As the PES loading increased, both the size and concentration of the

dispersed PES particles increased accordingly. Figure 2 illustrates the size distribution of these heterogeneous microphases in relation to the PES loading percentage. On the fractured surfaces of SENB specimens, the mean particulate radius was found to be 0.36, 0.61, 0.64, and 0.78 μm for P2.5, P5, P7.5, and P10, respectively. The formation of heterogeneous phase structures is sensitive to the conversion rate during the polymerization-induced phase-separation process [23]. The composition ratio of the coexisting constituents plays a crucial role in influencing the cloud-point conversions and interdiffusion coefficients before network formation [24].

The interaction between the cracks and the PES particles leads to the emergence of three toughening mechanisms, namely shear yielding, crack bridging, and crack deflections. At room temperature, shear yielding was the dominant mechanism, characterized by a tail-like matrix grazing and plastic void growth (Figure 1b-c), as the matrix is susceptible to yielding. The modulus mismatch between the PES and epoxy phases creates stress concentrations, which in turn forces the epoxy/PES interface to expand and undergo gradual shear behind the particles due to unbalanced strains [25]. This shear yielding mechanism helps in absorbing energy and retarding the crack propagation, thus contributing to the enhancement of the fracture toughness of the material.

Traces of plastically deformed PES particles indicate a possible role in bridging between the crack surfaces, adding more surface tractions. Crack bridging seems to be influenced by the void growth mechanism as some particles were pulled out from the matrix. This dependency was less obvious at 77 K since the matrix became more brittle and exhibited less void growth. Another potential explanation is attributed to the mismatch in the coefficients of thermal expansion (CTE) between the co-existing phases which, in turn, enhanced the interface interlocking strength. The CTE of epoxies ranges between 55-80 ppm/K, which is generally higher than the CTE of PES (50-60 ppm/K) [26-28]. As the testing temperature dropped, the matrix was more prone to shrink than the PES microphases.

At cryogenic temperatures, crack deflections were observed to occur, and these deflections became more prominent in P7.5 and P10 blends. These crack deflections were characterized by deviations in the main crack plane, indicating a transformation from the opening fracture Mode I to shearing Mode II. This shearing mode requires a more substantial amount of energy to propagate the crack. The presence of larger PES particulates in P7.5 and P10 blends potentially acted as impenetrable objects, leading to the observed crack deflections. In the case of P10, intact large particles caused out-of-plane crack deflections at 77 K. On the other hand,

in blends with smaller PES particulates, such as P2.5, snapping of the particles was more prone to occur, especially when there was a significant spacing between the obstacles. Overall, these observations demonstrate how the domain size and spacing between the PES particulates influence the toughening mechanisms at cryogenic temperatures.

Literature indicates that a co-continuous phase morphology exhibits greater toughening effects compared to the particulate morphology [25, 29]. This transition in the phase microstructure is influenced not only by the concentration of PES but also by its molecular weight and the curing temperature [23]. Previous studies have reported the presence of a dual-phase microstructure at various PES loadings, such as 10 phr [29], 15 phr [6, 23, 25, 30], and sometimes even beyond 20 phr [31]. Therefore, an attempt was made to create P15 specimens. However, it is important to mention that, during this process, difficulties arose as the blend with 15 phr PES became extremely viscous, resulting in challenges during the degassing and casting steps.

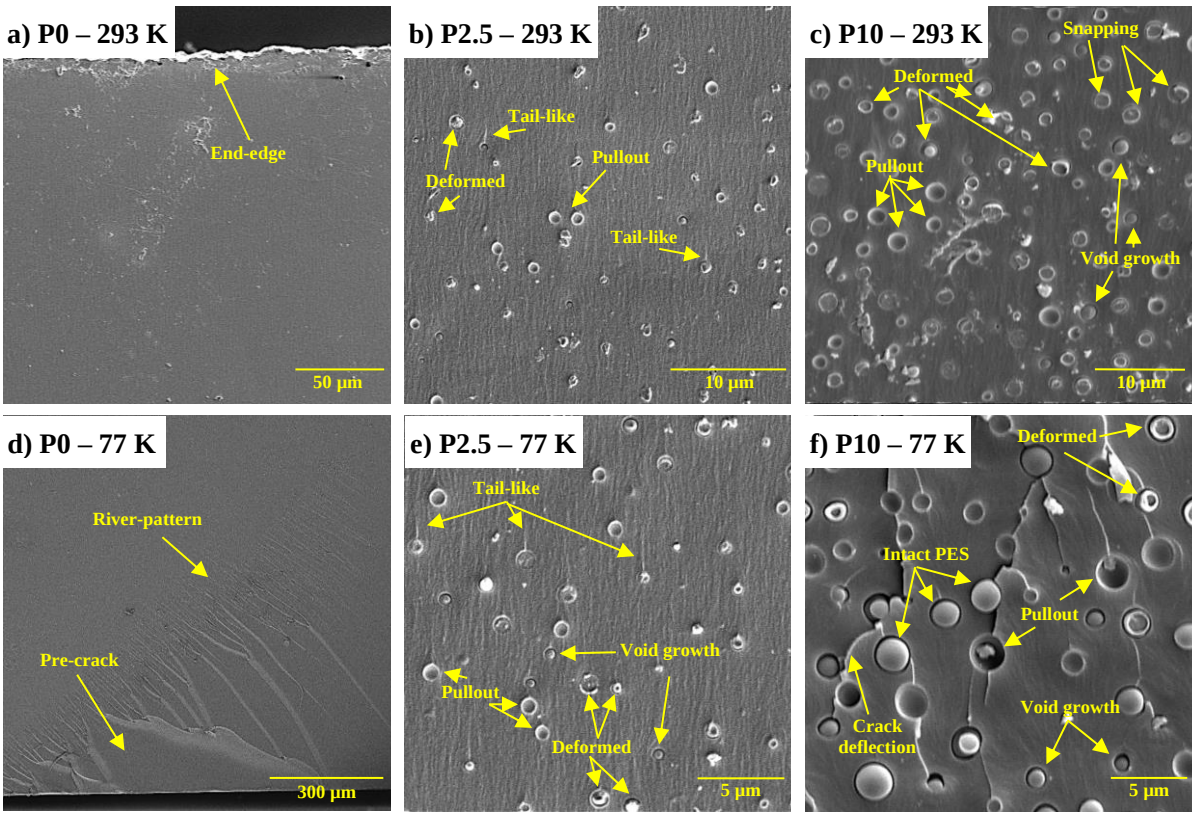

Figure 1. SEM photographs of SENB fractured surfaces of (a-d) pristine epoxy, (b,e) 2.5 phr, and (c,f) 10 phr PES-epoxy blends. The samples in (a-c) were fractured at room temperature (293 K) whereas the topologies in (d-f) are cryogenic (77 K) fractures. The direction of crack propagation is upward. Fracture images in P2.5 and P10 were taken far away from the pre-crack and edges.

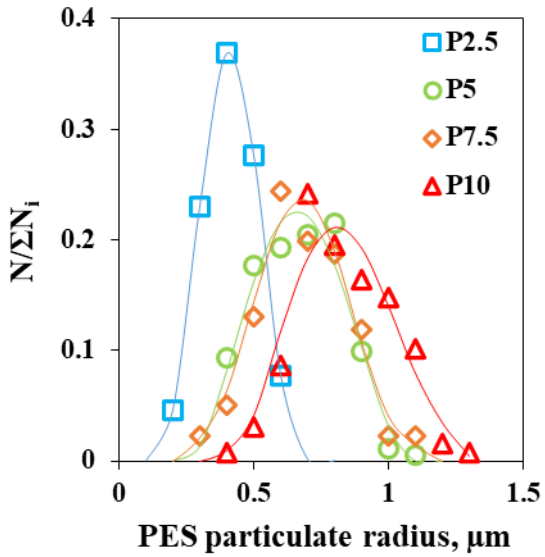

Figure 2. Size distribution of heterogeneous PES particulates observed on SENB fractured surfaces of 2.5-10 phr epoxy/PES blends.

The fractured surfaces of the P15 specimens, as shown in Figure 3, reveal a co-continuous phase morphology characterized by interconnected PES-rich and epoxy-rich domains with irregular shapes. The formation of these domains occurs without nucleation, but rather resulting from the spinodal decomposition mechanism of a thermodynamically unstable blend [24]. Each phase domain contains dispersions of the other phase, indicating that a secondary phase-separation process has taken place [23].

Within the co-continuous phase morphology, a particulate morphology is observed within the epoxy-rich domain (Figure 3b), while a nodular epoxy morphology is formed within the PES-rich phase (Figure 3c). The topology of the fractured surfaces appears very rough compared to the other samples, even at 77 K. This roughness suggests excessive shifts in the crack plane and potential plastic deformations of the PES-rich phase, contributing to the observed toughening effects in the P15 blend. Brooker et al. [31] also attempted to measure the fractured surface roughness versus PES concentration, but the samples with a bicontinuous phase morphology were too rough to obtain precise measurements.

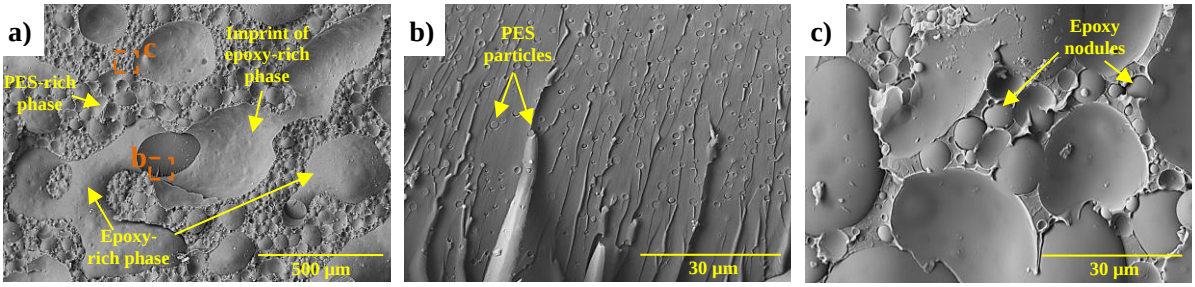

Figure 3. SENB fracture surfaces of a 15 phr epoxy/PES blend at 77 K, highlighting a) the co-continuous phase morphology, b) epoxy-rich phases containing PES particulates, and c) PES-rich phase with nodular epoxy morphology.

3.2 Fracture toughness of PES toughened epoxies

The fracture toughness (K_{Ic}) and critical strain energy release rates (G_{Ic}) of epoxy/PES blends with varying concentrations of 0, 2.5, 5, 7.5, 10, and 15 phr are illustrated in Figure 4. At room temperature, the measured K_{Ic} and G_{Ic} values for pristine epoxy resin (P0) were 0.708 MPa.m$^{1/2}$ and 0.149 kJ/m^2, respectively. However, the ability of P0 to resist crack propagation was found to be greater at 77 K, measuring approximately 1.5 times higher values at 1.727 MPa.m$^{1/2}$ for K_{Ic} and 0.384 kJ/m^2 for G_{Ic}. This increase in crack resistance at lower temperatures is attributed to the reduced mobility of polymer chains as the temperature drops, making the material harder to fracture [30]. This appears to be the main crack resistance mechanism in P0 as there is no evidence of contribution from plastic deformations on the fractured surface of P0 in Figure 1a.

At room temperature, higher levels of fracture toughness were achieved as the dispersion of PES particles increased. These results are in good agreement with findings from other studies [6, 25, 29, 30]. The most significant improvements in K_{Ic} and G_{Ic} at 293 K were observed in the P15 specimens, showing enhancements of 72% and 168%, respectively. Tangthana-umrung et al. [29], in a similar study using an epoxy resin system identical to the one in this research, reported even higher enhancements of 94% and 300% in K_{Ic} and G_{Ic}, respectively, at 15 phr PES loading. However, it is worth noting that the difference in curing schedules used in the two studies could account for the observed discrepancy in the extent of toughening improvements. The curing rate and temperature play a significant role in altering the developed phase morphologies in the epoxy/PES blends, and subsequently, these variations affect the fracture toughness enhancements.

The cryogenic fracture toughness properties of the epoxy/PES blends showed steady improvement with higher PES content until 10 phr. The highest fracture toughness was

observed at 10 phr, with K_{Ic} measuring 2.551 MPa.m$^{1/2}$ and G_{Ic} measuring 1.075 kJ/m^2. This represents a 48% improvement in K_{Ic} and 180% improvement in G_{Ic} compared to the P0. However, when the PES content was further increased to 15 phr, the G_{Ic} dropped by 24%, but it was still 156% higher than that of P0. However, P15 showed a slight 5% reduction in K_{Ic} compared to P0, indicating a lower intrinsic resistance to crack growth.

This discrepancy in behavior can be attributed to the temperature-dependent mechanical properties of the PES-rich domain. At room temperature, PES has a tensile strength of 89 MPa [32], which is 44% higher than the strength of the neat epoxy in this study [29]. Furthermore, PES is generally more ductile than epoxy resins, making it more ductile and able to dissipate more fracture energy through plastic deformation. Yang et al. [30] reported a 49% increase in the tensile failure strain of 15 phr epoxy/PES blends at 293 K, whereas 28% increase was measured at 77 K. As a result, both K_{Ic} and G_{Ic} are expected to improve with higher PES loading at room temperature.

At cryogenic conditions, however, the strength of the pure epoxy resin increased remarkably, as mentioned earlier, and this was the main cause of its resistance to crack propagation in P0. In blends with P2.5 to P10 loading, the crack had the option to propagate through the continuous phase of epoxy resin, and thus, K_{Ic} was not reduced. The dispersion of PES particles induced stress concentrations and crack deflections, leading to improved crack resistance. Consequently, the improvement in G_{Ic} is more pronounced than K_{Ic} due to the presence of crack bridging and plastic deformation of PES microphases in these blends.

In the case of P15, these mechanisms were also present at 77 K, as observed in Figure 3c, which contributed to the improvement in G_{Ic}. However, Figure 3a showed that the crack front generally advanced around, rather than through, the epoxy-rich domains. The epoxy-rich phase was mainly fractured at its narrow structure, leaving an imprint in the PES-rich domains (Figure 3a). This implies that there was less crack resistance through the PES-rich domain and, in turn, resulted in a reduction in K_{Ic} for a co-continuous phase morphology.

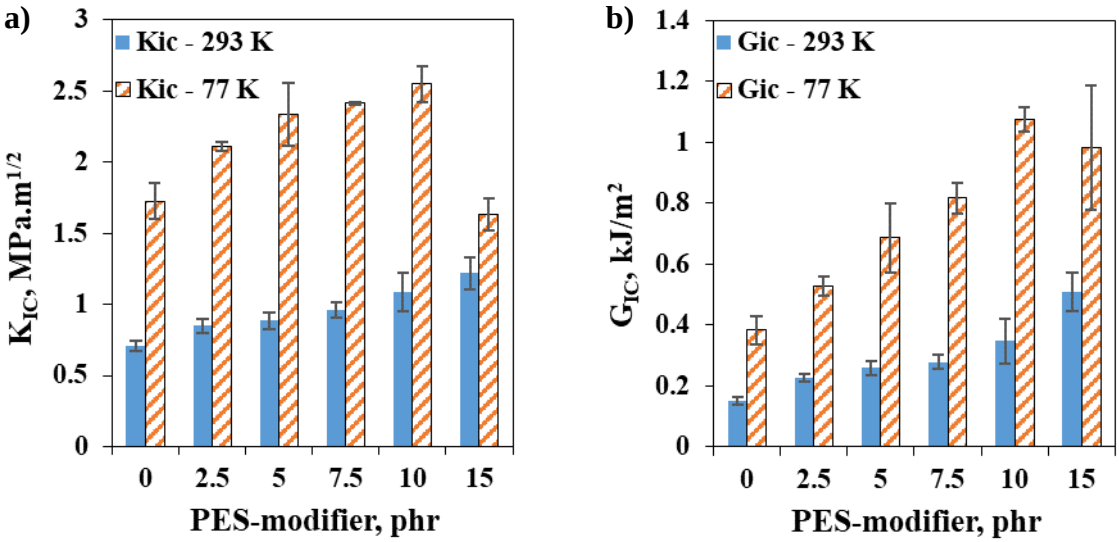

Figure 4. Improvements in the a) plane strain fracture toughness (K_{Ic}) and b) critical strain energy release rate (G_{Ic}) of SENB specimens as a function of PES mass loading, measured at 293 and 77 K.

3.3 Improvements in interlaminar fracture toughness

Figure 5 shows the morphology of the electrospun PES nanofibrous veil, which is beads-free and has an average diameter of 0.78 ± 0.24 µm. The electrospinning process continued for 5 minutes, resulting in the deposition of an approximately 5 µm thick PES veil with an areal weight of 0.6 gsm after drying onto one face of a carbon fabric.

The mechanical performance of the PES interleave was compared to other laminates that were impregnated with 5, 7.5, and 10 phr epoxy/PES blends. The 2.5 phr blend was excluded from this part of the study because it showed relatively slight improvements in the fracture toughness properties of the epoxy resin compared to the blends with higher PES concentrations. Additionally, the 15 phr epoxy/PES blend had an excessively high viscosity, making it impractical to impregnate the carbon fabric and, therefore, it was excluded from this part of the study.

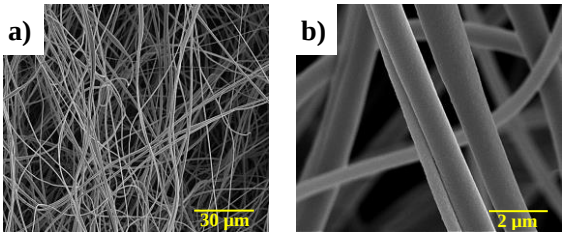

Figure 5. SEM images of electrospun polyethersulfone nanofibres. a) displays the beads-free morphology of the nanofibres and b) shows average diameter of 0.78 µm.

Figure 6 shows representative load versus crack opening displacement curves from the DCB fracture test conducted at both 293 K and 77 K temperatures. The curves exhibit a typical linear elastic behavior up to the maximum load, which denotes the onset of failure at the insert. At cryogenic temperatures, the variation in the load compliance between the laminates is more apparent than at room temperature. The interleaved laminate (P-Veil) displayed a maximum change of -17.6% compared to the baseline laminate (P0). This variation can be attributed to slight differences in the laminates' thickness (± 0.18 mm) and potentially the influence of PES dispersion on the overall mechanical response of the laminates [29, 30].

Overall, the load carrying capacity of toughened laminates is remarkably higher than the baseline laminate. The maximum load sustained by the baseline laminate was 44 and 41 N at 293 and 77 K, respectively. The incorporation of PES-modifier effectively delayed the onset of delamination at room temperature due to increased plasticity and energy dissipation. The greatest load peak at 293 K was observed in P7.5, measuring 64 N, which is 45% higher than P0. The P-Veil specimen achieved a peak load of 62 N at 293 K, while P10 measured 59 N. In other words, the performance of the P-Veil specimen lies mostly between the curves of P7.5 and P10 specimens.

The crack propagation at room temperature was more stable compared to its growth under a cryogenic test condition. The crack advanced rapidly by 1-2 mm at 293 K, while at 77 K, it grew significantly faster, in the order of 3-8 mm. At cryogenic temperatures, the observed zigzag pattern in all the curves in Figure 6b indicates the presence of a stick-slip fracture mechanism. The peak loads of the laminates overlap and are mostly observed at the second peak in the zigzag trend. This is potentially because the crack initially grew steadily during the stick phase and then got arrested during the slip phase, leading to similar load peaks for the different laminates.

The inherent brittle behavior of the matrix at lower temperatures creates an imbalance between the energy dissipation mechanisms at the crack tip and the applied loading [35]. The pure epoxy matrix exhibited more excessive and unstable crack advancement (slip) compared to the toughened samples. In contrast, all the toughened samples showed more stable crack advancement and fewer drops at the applied load level. This indicates that the crack tip is more frequently arrested due to its interaction with the dispersed PES particles [33]. Cheng et al. [34] noticed a transition in the curve behavior from a zigzag shape to a smooth wave-like trend as the PES interleave thickness increased. Similarly, Quan et al. [35] reported a 33% slower crack growth rates through interleaved laminates compared to the benchmark laminate, resulting in smoother load-displacement curves.

The delamination resistance curves shown in Figure 7 exhibit a significant R-curve effect in a rising manner, regardless of the testing temperature. This behavior is an artefact in unidirectional laminates and is attributed to the presence of fibre bridging, which extends the length of the damage process zone [36]. A similar observation was made by Quan et al. [35], who reported a plateau in the R-curves for interleaved unidirectional laminates at a crack length beyond 75 mm.

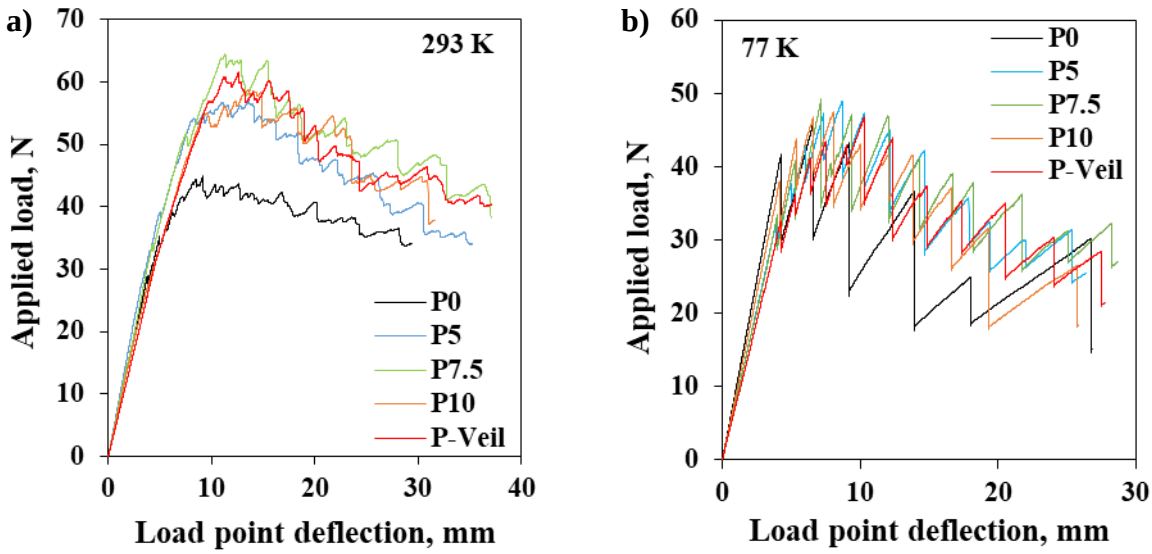

Figure 6. DCB Load-displacement curves of toughened composite laminates with epoxy/PES blends with 5, 7.5, and 10 phr and a 5 µm thick PES interleave: a) at room temperature and b) at cryogenic temperature.

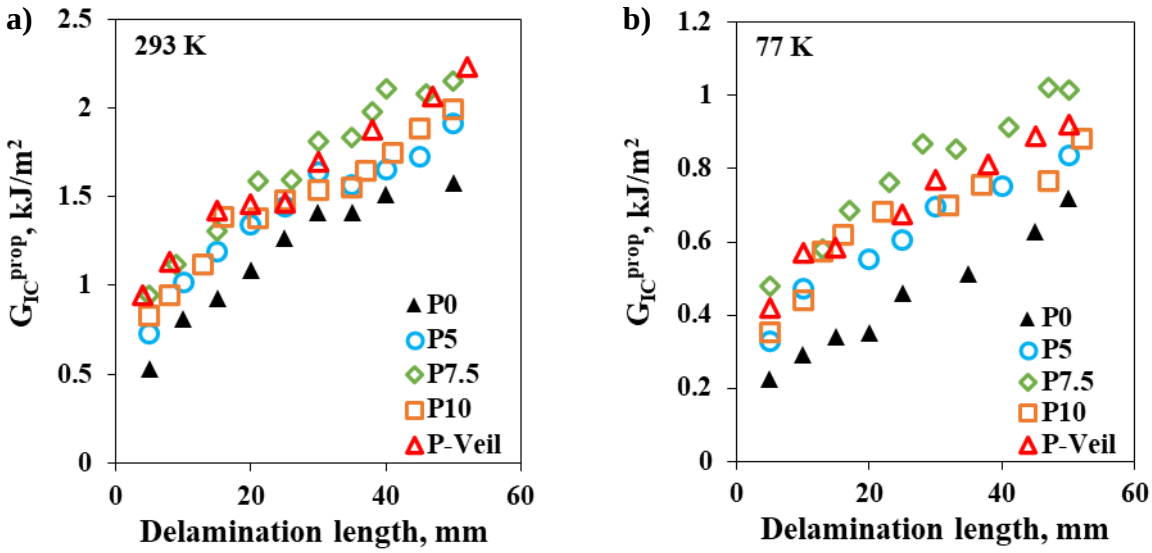

Figure 7. Delamination resistance curves obtained from a DCB test arrangement carried out at a) room temperature and b) cryogenic temperature.

Figure 8 displays the averaged values of Mode I critical strain energy release rate (G_{Ic}^{ini}) and the crack propagation energy (G_{Ic}^{prop}) of the composite laminates at both 293 and 77 K temperatures. The G_{Ic}^{prop} values were calculated by averaging the values obtained with a delamination length beyond 40 mm, as the R-curve trend kept on rising. In general, all the toughened laminates demonstrated improvements in G_{Ic}^{ini} and G_{Ic}^{prop} compared to the unmodified laminate. At room temperature, the improvements in G_{Ic}^{ini} with 5, 7.5, and 10 phr PES concentrations were 29%, 79%, and 45%, respectively. However, at cryogenic temperature, these laminates exhibited lesser toughening levels, with G_{Ic}^{ini} improvements of 20%, 48%, and 28% for the P5, P7.5, and P10, respectively. On the other hand, the incorporation of a PES veil significantly enhanced G_{Ic}^{ini} by 76% and 48% at 293 and 77 K, respectively. This indicates that the interleaving technique provides greater toughening effects compared to the epoxy/PES blends at cryogenic temperatures.

The enhancements in the G_{Ic}^{prop} with PES-modifiers are less pronounced than G_{Ic}^{ini}, as they are approximately half the improvement levels. The measured G_{Ic}^{prop} values of the unmodified laminate at 293 and 77 K are 1.5 and 0.7 kJ/m^2, respectively. The best improvements in G_{Ic}^{prop} at 293 K is recorded with P7.5 laminate, showing a value of 2.1 kJ/m^2. On the other hand, P-Veil exhibited the greatest G_{Ic}^{prop} of 0.91 kJ/m^2 at 77 K. The maximum difference in the measurements between P7.5 and P-Veil specimens is 6%, which suggests that the formed phase morphology with the 5 µm interleave is similar to that of the P7.5 epoxy/PES blend.

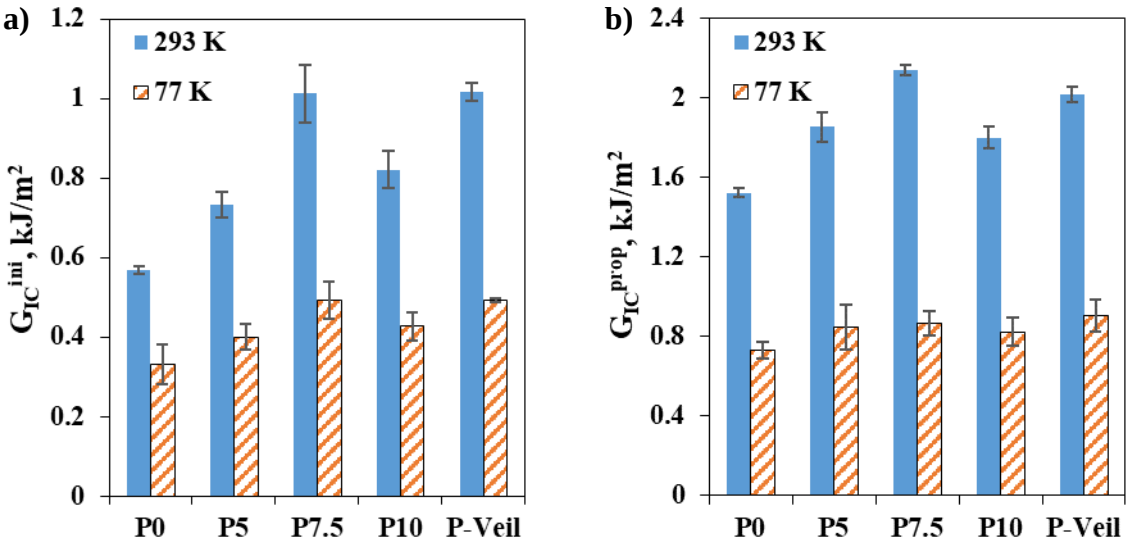

Figure 8. Improvements in a) the Mode I critical strain energy release rate (G_{Ic}^{ini}) and b) the crack propagation energy (G_{Ic}^{prop}) of composite laminates at room (293 K) and cryogenic (77 K) temperatures.

3.4 Fractography and Synergistic Toughening Mechanism

Representative SEM images of the fracture surfaces of DCB samples are illustrated in Figure 9. Across all the toughened laminates at both 293 and 77 K, smooth imprints of the fibres are clearly visible, indicating the presence of excessive fibre bridging. This observation explains the rising behavior of the measured R-curves, where fibre bridging extends the length of the damage process zone, leading to enhanced fracture toughness.

The fracture surface of the control sample (P0) exhibits a typical saw-teeth shape fracture, which is a common feature of brittle fractures. In contrast, the toughened laminates display the particulate phase morphology, similar to the microstructures observed on SENB fractures. This confirms that the PES particles became miscible in the epoxy resin and subsequently phase-separated during the curing reaction.

The fracture surfaces of the toughened samples appear rougher and exhibit more features due to the inclusion of PES microphases. Signs of crack deflections, void growth, and PES particle deformation and debonding are visible in Figure 9b-i. In addition, subsurface matrix fracture occurred beneath the exposed fibres during the fracture process, indicating significant shifts in the main crack plane. Broken fibres (Figure 9i) were observed on the cryogenic fractures of P-Veil, suggesting crack path migration. These toughening mechanisms contributed to more arrests in crack propagation and led to substantial improvements in G_{Ic}^{ini} and G_{Ic}^{prop}.

It is important to note that large and intact PES particles were observed on cryogenic fractures, as seen in the SENB fracture of P10 (Figure 1f). These particles tend to be larger and less uniform compared to the PES-modified blends. Additionally, fractured surfaces of P7.5 and P10 exhibited a co-continuous PES-rich phase with embedded epoxy nodules, as shown in Figure 9g and Figure 9h. This behavior might be influenced by the presence of fibre reinforcements, which could have restricted the phase-separation of highly concentrated PES during the curing reaction. Another possible explanation is the localized temperature variation during the laminate curing process. Phase-separation at lower temperatures may result in a co-continuous phase morphology for the epoxy resin system used in this study when the PES concentration exceeds 5 phr, as reported in [29]. This phenomenon could explain the superior interlaminar toughening effects of P7.5 over P10. With higher PES loading, more PES-rich domains will tend to form, leading to lower crack resistance, as previously observed in the bulk P15 performance.

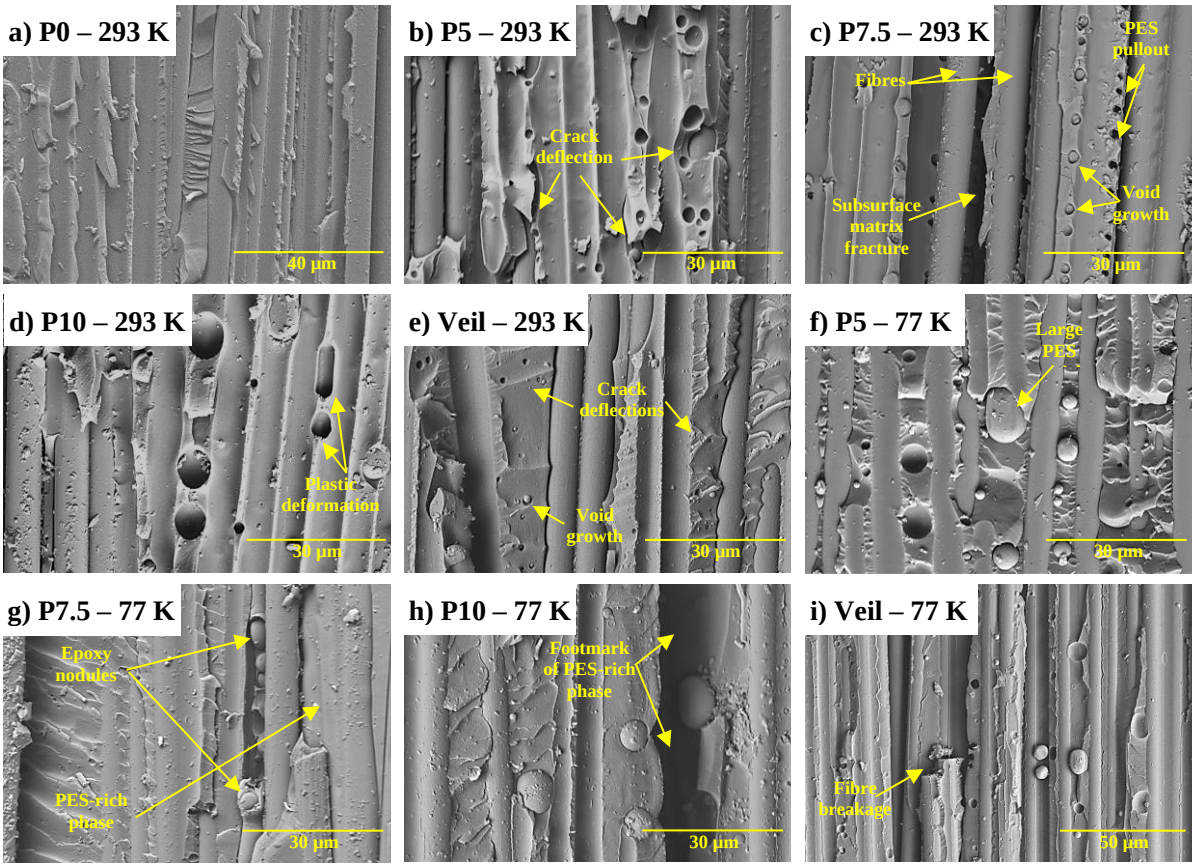

Figure 9. SEM images of DCB fractured surfaces at a-e) room temperature 293 K and f-i) cryogenic temperature 77 K.

4 Conclusions

The study investigated the influence of PES loading on the phase microstructure and mechanical performance of an epoxy-anhydride thermoset. As the PES concentration exceeded 10 phr, a transition from a particulate microstructure to a network of co-continuous phases was observed. SENB tests demonstrated consistent improvements in performance with increasing PES loading at room temperature. The most significant enhancements in K_{Ic} and G_{Ic} at 293 K were at 72% and 168%, respectively, with 15 phr epoxy/PES blend. However, at cryogenic temperatures, the 10 phr blend outperformed the 15 phr blend, with improvements of 48% in K_{Ic} and 180% in G_{Ic} compared to the neat epoxy resin. This difference in cryogenic performance was attributed to the co-continuous phase morphology, which allowed the crack front to advance around, rather than through, the epoxy-rich domains.

The electrospun PES nanofibres exhibited bead-free morphology, with an average diameter of 0.78 μm. Incorporating the PES veil into the composite laminate resulted in a significant enhancement of the Mode I critical strain energy release rate (G_{Ic}^{ini}) by 76% and 48% when tested at 293 K and 77 K, respectively. Additionally, the Mode I crack propagation energy (G_{Ic}^{prop}) was also increased by 33% and 24% at 293 K and 77 K, respectively. Comparing the performances of the interleaved laminate and the toughened laminate with 7.5 phr PES loading, the results showed close similarity, with a maximum variation of only 6% in the measurements. These improvements in interlaminar fracture toughness were attributed to the unique synergistic effects of the dispersed PES particulates. Moreover, the fracture surfaces of the DCB samples revealed the presence of multiple toughening mechanisms, including crack deflections, void growth, crack bridging, and subsurface matrix fracturing. These mechanisms further contributed to the enhanced fracture toughness observed in the materials.

5 References

1. Hohe, J., et al., *Performance of fiber reinforced materials under cryogenic conditions—A review.* Composites Part A: Applied Science and Manufacturing, 2020: p. 106226.
2. Yates, B., et al., *The thermal expansion of carbon fibre-reinforced plastics.* Journal of Materials Science, 1979. **14**(5): p. 1207-1217.
3. He, Y.-x., et al., *Micro-crack behavior of carbon fiber reinforced thermoplastic modified epoxy composites for cryogenic applications.* Composites Part B: Engineering, 2013. **44**(1): p. 533-539.
4. Korokhin, R., et al., *Rheological and physicomechanical properties of epoxy-polyetherimide compositions.* Mechanics of Composite Materials, 2015. **51**: p. 313-320.
5. Chen, H., et al., *Mechanical properties of reactive polyetherimide-modified tetrafunctional epoxy systems.* Polymer, 2023. **270**: p. 125763.
6. Jiang, M., et al., *Enhanced mechanical and thermal properties of monocomponent high performance epoxy resin by blending with hydroxyl terminated polyethersulfone.* Polymer Testing, 2018. **69**: p. 302-309.
7. Cheng, X., et al., *Morphologies and mechanical properties of polyethersulfone modified epoxy blends through multifunctional epoxy composition.* Journal of Applied Polymer Science, 2017. **134**(18).
8. Cheng, C., et al., *Improving the interlaminar toughness of the carbon fiber/epoxy composites via interleaved with polyethersulfone porous films.* Composites Science and Technology, 2019. **183**: p. 107827.
9. Solodilov, V. and Y.A. Gorbatkina, *Properties of unidirectional GFRPs based on an epoxy resin modified with polysulphone or an epoxyurethane oligomer.* Mechanics of composite materials, 2006. **42**: p. 513-526.
10. Sun, Z., et al., *Enhancing the mechanical and thermal properties of epoxy resin via blending with thermoplastic polysulfone.* Polymers, 2019. **11**(3): p. 461.
11. Jin, H., et al., *Fracture toughness and surface morphology of polysulfone-modified epoxy resin.* Journal of Industrial and Engineering Chemistry, 2015. **25**: p. 9-11.
12. Deng, S., et al., *Thermoplastic–epoxy interactions and their potential applications in joining composite structures–A review.* Composites Part A: Applied Science and Manufacturing, 2015. **68**: p. 121-132.
13. Rico, M., et al., *Phase separation and morphology development in a thermoplastic-modified toughened epoxy.* European polymer journal, 2012. **48**(10): p. 1660-1673.
14. Zhang, J., T. Lin, and X. Wang, *Electrospun nanofibre toughened carbon/epoxy composites: Effects of polyetherketone cardo (PEK-C) nanofibre diameter and interlayer thickness.* Composites science and technology, 2010. **70**(11): p. 1660-1666.
15. Surendran, A., et al., *An overview of viscoelastic phase separation in epoxy based blends.* Soft Matter, 2020. **16**(14): p. 3363-3377.
16. Li, H., et al., *Polyetherketone powder/epoxy blends with low viscosity and high mechanical properties.* High Performance Polymers, 2020. **32**(9): p. 1052-1060.
17. Li, G., et al., *Inhomogeneous toughening of carbon fiber/epoxy composite using electrospun polysulfone nanofibrous membranes by in situ phase separation.* Composites Science and Technology, 2008. **68**(3-4): p. 987-994.
18. Daelemans, L., et al., *Damage-resistant composites using electrospun nanofibers: a multiscale analysis of the toughening mechanisms.* ACS applied materials & interfaces, 2016. **8**(18): p. 11806-11818.
19. Kohlman, L., *Engineered Polymer Composites Through Electrospun Nanofiber Coating of Fiber Tows*. 2014, NASA.

20. Shakil, U.A., et al., *Mechanical properties of electrospun nanofiber reinforced/interleaved epoxy matrix composites—A review.* Polymer Composites, 2020. **41**(6): p. 2288-2315.
21. Zhang, J., et al., *Phase morphology of nanofibre interlayers: critical factor for toughening carbon/epoxy composites.* Composites science and technology, 2012. **72**(2): p. 256-262.
22. Tsang, W.L. and A.C. Taylor, *Fracture and toughening mechanisms of silica-and core–shell rubber-toughened epoxy at ambient and low temperature.* Journal of Materials Science, 2019. **54**(22): p. 13938-13958.
23. Shapagin, A.V., et al., *Phase equilibrium, morphology, and physico-mechanics in epoxy–thermoplastic mixtures with upper and lower critical solution temperatures.* Polymers, 2020. **13**(1): p. 35.
24. Tercjak, A., *Phase separation and morphology development in thermoplastic-modified thermosets*, in *Thermosets*. 2018, Elsevier. p. 147-171.
25. Jung, H.-S., et al., *Evaluation of the mechanical properties of polyether sulfone-toughened epoxy resin for carbon fiber composites.* Fibers and Polymers, 2021. **22**: p. 184-195.
26. Sun, Q., et al., *High performance epoxy resin with ultralow coefficient of thermal expansion cured by conformation-switchable multi-functional agent.* Chemical Engineering Journal, 2022. **450**: p. 138295.
27. Chun, H., et al., *Preparation of low-CTE composite using new alkoxysilyl-functionalized bisphenol A novolac epoxy and its CTE enhancement mechanism.* Polymer, 2020. **207**: p. 122916.
28. Van den Berg, D., et al., *Hygroscopic and thermal micro deformations of plastic substrates for flexible electronics using digital image correlation.* Polymer testing, 2011. **30**(2): p. 188-194.
29. Tangthana-umrung, K., X. Zhang, and M. Gresil, *Synergistic toughening on hybrid epoxy nanocomposites by introducing engineering thermoplastic and carbon-based nanomaterials.* Polymer, 2022. **245**: p. 124703.
30. Yang, G., et al., *Preparation and cryogenic mechanical properties of epoxy resins modified by poly (ethersulfone).* Journal of Polymer Science Part A: Polymer Chemistry, 2008. **46**(2): p. 612-624.
31. Brooker, R., A. Kinloch, and A. Taylor, *The morphology and fracture properties of thermoplastic-toughened epoxy polymers.* The Journal of Adhesion, 2010. **86**(7): p. 726-741.
32. Li, F., et al., *Enhanced mechanical properties of short carbon fiber reinforced polyethersulfone composites by graphene oxide coating.* Polymer, 2015. **59**: p. 155-165.
33. Zhou, J., et al., *Synergetic improvement of interlaminar fracture toughness in carbon fiber/epoxy composites interleaved with PES/PEK-C hybrid nanofiber veils.* Advanced Fiber Materials, 2022. **4**(5): p. 1081-1093.
34. Cheng, C., et al., *Simultaneously improving mode I and mode II fracture toughness of the carbon fiber/epoxy composite laminates via interleaved with uniformly aligned PES fiber webs.* Composites Part A: Applied Science and Manufacturing, 2020. **129**: p. 105696.
35. Quan, D., et al., *Interlaminar fracture toughness of aerospace-grade carbon fibre reinforced plastics interleaved with thermoplastic veils.* Composites Part A: Applied Science and Manufacturing, 2020. **128**: p. 105642.
36. Meireman, T., et al., *Nanofibre toughening of dissimilar interfaces in composites.* Materials & Design, 2020. **195**: p. 109050.